Expression of cell type incongruent alpha-cardiac actin 1 subunit in medulloblastoma reveals a novel mechanism for cancer cell survival and control of migration

Rahul Suresh, Daniel Picard, Rita Lo, Jamie Beaulieu, Marc Remke, and Roberto Jose Diaz

Montreal Neurological Institute, McGill University, Montreal, Québec, Canada (R.S., R.L., J.B., R.J.D.); Division of Pediatric Neuro-Oncogenomics, German Cancer Research Center (DKFZ), Heidelberg, Germany (D.P., M.R.); German Consortium for Translational Cancer Research (DKTK), partner site Essen/Düsseldorf, Düsseldorf, Germany (D.P., M.R.); Department of Pediatric Oncology, Hematology, and Clinical Immunology, Medical Faculty, Heinrich Heine University (HHU), University Hospital Düsseldorf (UKD), Düsseldorf, Germany (M.R.); Department of Neuropathology, Medical Faculty, HHU, UKD, Düsseldorf, Germany (M.R.). Department of Neurology and Neurosurgery, Montreal Neurological Institute and Hospital, Faculty of Medicine, McGill University, Montreal, Québec, Canada (R.J.D.)

Corresponding Author: Roberto Jose Diaz, MD, PhD, FRCSC, Department of Neurology and Neurosurgery, Montreal Neurological Institute and Hospital, 3801 Rue University, Montreal, Quebec, H3A 2B4, Canada (roberto.diaz@mcgill.ca).

Abstract

Background. Alterations in actin subunit expression have been reported in multiple cancers, but have not been investigated previously in medulloblastoma.

Methods. Bioinformatic analysis of multiple medulloblastoma tumor databases was performed to profile *ACTC1* mRNA levels. Western blot was used to verify protein expression in established medulloblastoma cell lines. Immunofluorescence microscopy was performed to assess ACTC1 localization. Stable cell lines with ACTC1 overexpression were generated and shRNA knockdown of ACTC1 was accomplished. We used PARP1 cleavage by Western blot as a marker of apoptosis and cell survival was determined by FACS viability assay and colony formation. Cell migration with overexpression or knockdown of ACTC1 was determined by the scratch assay. Stress fiber length distribution was assessed by fluorescence microscopy.

Results. *ACTC1* mRNA expression is highest in SHH and WNT medulloblastoma among all subgroups. ACTC1 protein was confirmed by Western blot in SHH subgroup and Group 3 subgroup cell lines with the lowest expression in Group 3 cells. Microscopy demonstrated ACTC1 co-localization with F-actin. Overexpression of ACTC1 in Group 3 cells abolished the apoptotic response to Aurora kinase B inhibition. Knockdown of ACTC1 in SHH cells and in Myc overexpressing SHH cells induced apoptosis, impaired colony formation, and inhibited migration. Changes in stress fiber length distribution in medulloblastoma cells are induced by alterations in ACTC1 abundance.

Conclusions. Alpha-cardiac actin (ACTC1) is expressed in SHH medulloblastoma. Expression of this protein in medulloblastoma modifies stress fiber composition and functions in promoting resistance to apoptosis induced by mitotic inhibition, enhancing cell survival, and controlling migration.

Key Points

- Alpha cardiac actin (ACTC1) is expressed in SHH and WNT medulloblastoma.
- ACTC1 incorporates into F-actin and confers resistance to apoptosis.
- ACTC1 is involved in control of survival and migration in SHH medulloblastoma.

Importance of the Study

Alpha-cardiac actin 1 (ACTC1), which is normally expressed in cardiac muscle, was found to be aberrantly expressed in medulloblastoma with higher levels expressed in WNT and SHH subtypes compared to Group 3 and Group 4. We demonstrate that ACTC1 incorporates into F-Actin and renders medulloblastoma cells resistant to apoptosis induced by mitotic inhibitor. Additionally, ACTC1 is involved in control of survival and migration in SHH cells with or without MYC overexpression. Our study shows for the first time that actin subunit composition alters stress fiber dynamics and contributes to tumorigenicity in medulloblastoma. This may have important implications in other primary brain cancers that demonstrate aberrant actin subunit expression such as glioblastoma.

The actin cytoskeleton and actin binding proteins play an important role in mechanisms of apoptosis in both normal cells and neoplastic cells.[1,2] Apoptosis can be stimulated by changes in actin polymerization[3–5]; by alteration of apoptosis regulating actin binding protein interaction; or by disruption of tropomyosin interactions with F-actin.[2,6] Alterations in actin subunit composition can also have effects on cell morphology, migration, and growth.[7–9] It has been previously reported that sonic hedgehog (SHH) medulloblastoma cells are resistant to apoptosis when mitosis is inhibited with a specific inhibitor of Aurora kinase B, whereas Group 3 cells demonstrated marked apoptosis.[10] The contribution of actin subunit expression to resistance to mitotic inhibition and migration in medulloblastoma cells is not known. We do know that F-actin plays a critical role in granule cell precursor migration[11] and that SHH medulloblastoma cells show gene expression profiles of developing granule cell precursors.[12] Abnormal expression of the alpha cardiac actin (ACTC1) actin subunit has been documented in multiple cancer types including head and neck,[13] urothelial,[14] prostate,[15] and glioblastoma.[16] Furthermore, *ACTC1* expression is upregulated in multi-drug-resistant breast cancer cells[17] and in lung cancer cells that survive exposure to paclitaxel.[18]

We hypothesized that ACTC1 expression in medulloblastoma could alter F-actin composition, thereby conferring an anti-apoptotic function in response to mitotic inhibition in medulloblastoma cells. Identification of resistance mechanisms in medulloblastoma subgroups is crucial since it is often difficult to treat at recurrence. The identification of pro-tumorigenic factors is essential for the development of more effective targeted therapy that will impair tumor growth, reduce migration and ultimately enhance patient survival with minimal toxic side effects.

Materials and Methods

Details for each method are provided in Supplementary Methods.

Cell Culture

SHH cells (DAOY, UW426, UW228) and their derivatives were grown as adherent cultures. Group 3 cells (D425, D458) were grown as suspension cultures. The UW426-Myc and UW228-Myc cell lines were provided by Dr. Annie Huang, The Hospital for Sick Children, and were originally derived by retroviral transduction to express higher levels of Myc protein compared to parental.[19] The D425 and D458 cells were kindly provided by Dr. Darell D. Bigner, Duke University.

Gene Expression Profiling in Cell Culture

Total RNA was isolated form UW426 and UW426-Myc cells exposed to vehicle control (0.01% v/v DMSO) or 100 nM AZD1152-HQPA Aurora kinase B inhibitor. The cRNAs generated were hybridized onto the Human HT-12 v4.0 BeadChip. The BeadChip was stained as per Illumina protocol and scanned on the iScan (Illumina). The data files were quantified in GenomeStudio Version 2011.1 (Illumina). To identify differentially expressed genes, linear models were fitted using the limma package (v3.12). The *t*-statistics derived from prespecified contrasts were moderated by empirical Bayes shrinkage. The moderated *t*-statistics were subsequently used for hypothesis testing and for Gene Set Enrichment Analyses. Microarray data, methods, and analysis have been uploaded to GEO (GSE159385). Gene enrichment maps were generated as described by Merico et al.[20] using conservative thresholds.

ACTC1 Analysis in Published Medulloblastoma Tumor Datasets

Previously published gene expression data were analyzed using R2 platform (https://hgserver1.amc.nl/cgi-bin/r2/main.cgi, Academic Medical Center (AMC) Amsterdam, Netherlands)). *ACTC1* was analyzed in multiple Medulloblastoma datasets (Heidelberg [PMID: 21911727], Pomeroy [PMID: 21098324], Cavalli/Remke [PMID: 28609654], Kool [PMID: 18769486], and Gilbertson [PMID: 22722829]) by subgroups that were assigned in the original publication. Additionally, a multi-cancer RNA sequencing dataset in R2 (Mixed Pediatric Pan Cancer - Pfister - 272 - FPKM - informp3) was analyzed to show ACTC1 in Medulloblastoma subgroups as well as across other CNS and non-CNS tumors. Neuroblastoma and T-ALL with a single datapoint were removed. ANOVA was used to calculate significance. Pearson correlation was used to determine the correlation between the expression

and methylation of *ACTC1* in the Cavalli/Remke dataset. Chromosome 15 copy number information was provided in the original publication for Cavalli/Remke and significance was calculated using ANOVA.

Quantitative RT-PCR

MB cell lines (UW426, UW426-Myc) were exposed to 0.01% DMSO or 100 nM AZD1152-HQPA for 48 h (Selleckchem). Total RNA was isolated and reverse transcription was performed on 100 ng of total RNA using random hexamer priming. Quantitative PCR using *ACTC1*-specific primers was performed and data analysis was performed using the Livek method. The experiment was conducted in 3 biological replicates and 4 technical replicates per run for each cell line.

Creation of Stable ACTC1-Overexpression Lines

SHH (UW426, UW426-Myc) cells were transfected plasmid DNA using Lipofectamine 2000 (ThermoFisher Scientific). For D458 cells, transfections were performed via electroporation instead. Forty-eight hours after transfection, selection was done for all cell lines using hygromycin. A single clone was then picked and expanded. The cells were transfected with either a human ACTC1 overexpression plasmid containing a C-terminal FLAG-tag (Ref.# HG10960-CF, Sino Biological), or an empty vector control. Expression of the plasmid transgene was confirmed by Western blot (WB) analysis for the FLAG tag.

Transient shRNA ACTC1 Knockdown

Transfection of shRNA expression plasmids were performed using Lipofectamine 2000 (ThermoFisher Scientific) reagent. The cells were transfected with either an ACTC1 knockdown DNA plasmid (GeneCopoeia; Cat# HSH018117-CH1) or a scrambled control (GeneCopoeia; Cat# CSHCTR001-CH1). The knockdown was confirmed by WB analysis.

Western Blot

Cell lysates were obtained using RIPA lysis buffer that was modified to contain a protease inhibitor.[21] Lysates from control liver and heart were obtained from mouse samples flash frozen in liquid nitrogen. Proteins were separated by SDS-PAGE on 10% gels and transferred to nitrocellulose membranes using a semi-dry transfer apparatus (Bio-Rad). The membranes were incubated with primary antibody at 4°C overnight followed by incubation with horseradish peroxidase-conjugated secondary antibody for 1 h, The following antibodies and dilutions were used: anti-ACTC1 (Cell Signaling Technologies) 1:1000, anti-PARP1 (Cell Signaling) 1:1000, anti-GAPDH (Cell Signaling) 1:1000, anti-Aurora Kinase B (Cell Signaling) 1:1000, anti-beta Actin (Abcam; ab115777) 1:1000. Secondary antibodies used were anti-rabbit or anti-mouse IgG conjugated to horseradish peroxidase (Cell Signaling) at a 1:2000 to 1:30,000 dilution.

FACS Cell Viability Assay

Cells were transfected with either a mock transfection, scrambled control, or ACTC1 knockdown plasmid 4 days prior to exposure to 100 nM AZD1152-HQPA (Selleck Chemicals LLC) or 0.01% v/v DMSO (Sigma) for 48 h. Cells were then stained with LIVE/DEAD® Fixable Aqua Dead Cell Kit (ThermoFisher Scientific) according to the manufacturer's protocol and analyzed on flow cytometer. For each experimental condition, 20,000–150,000 cells were analyzed in 3 independent trials. An Attune NxT flow cytometer (ThermoFisher Scientific) was used with Attune NxT software. Data analysis was conducted with FCS Express 7 (De Novo Software).

Colony Formation Assay

The cells were allowed to grow in standard culture media with the media being changed every 3 days. After 5 days (UW426-Myc) or 7 days (UW426) of growth, the colonies were stained with crystal violet solution. The number of colonies per well was counted using a dissecting microscope with a minimum of 50 cells necessary to constitute a colony.

Wound Closure Assay

Cells were cultured in a confluent monolayer. The media was changed to a serum-free media and a scratch was created in the well with a 200-μL pipette tip. Phase-contrast imaging was done at 0, 12, and 24 h, and the diameter of the wound was measured using ImageJ software. Seven different points were measured along the scratch.

Immunofluorescence

Cells were seeded on a sterile glass coverslip and fixed with 4% paraformaldehyde. After blocking, incubations were done with primary antibodies overnight at 4°C, and with secondary antibodies for 1 h. The following antibodies and dilutions were used: anti-ACTC1 (Cell Signaling Technologies) 1:1000, anti-FLAG (Sigma Aldrich Canada Ltd.) 1:500. Secondary antibodies used were Alexa-Fluor 488 nm anti-rabbit IgG (Life Technologies Inc.) or Alexa-Fluor 488 anti-mouse IgG (Life Technologies Inc.) at a 1:500 dilution. Each coverslip was incubated in 1U of Alexa-Fluor 647 nm fluorescent Phalloidin (ThermoFisher Scientific) and in Hoechst nuclear stain (ThermoFisher Scientific) at a 1:4000 dilution. The coverslips were then imaged using a Zeiss LSM700 confocal microscope with Zen Black 2010 acquisition software (Carl Zeiss).

Stress Fiber Analysis

Cells were stained with Alexa-Fluor 647 nm fluorescent Phalloidin (ThermoFisher Scientific) and Hoechst 177 nuclear stain (ThermoFisher Scientific). Images were acquired using a Zeiss LSM700 confocal microscope with Zen Black 2010 acquisition software (Carl Zeiss). Stress

fibers were analyzed using FSegment (Universitätsmedizin Greifswald) software in MATLAB Runtime (MathWorks) according to the protocol by Rogge et al.[22] and using the parameters listed in Supplementary Table 1. Images of at least 150 cells were taken for each cell line in 3 independent trials. 1 pixel length was equivalent to 0.1 μm.

Statistics

Prism 8 (GraphPad Software, Inc.) was used for statistical analysis. All measures are reported as mean ± standard error. Means were compared by independent samples Student's t-test. A P-value less than .05 was selected for significance. Unless otherwise indicated, all experiments were averaged for 3 independent trials.

Results

ACTC1 Expression in Medulloblastoma Varies with Subgroup Type

Alpha-cardiac actin 1 (ACTC1) is an actin isoform that is primarily found in cardiac tissue. Here we demonstrate that ACTC1 is also expressed in medulloblastoma. Analysis of 5 independent medulloblastoma tumor gene expression data sets demonstrated higher *ACTC1* mRNA expression in SHH and WNT tumors compared to Group 3 or Group 4 tumors (Figure 1A, Supplementary Figure 1A–D). *ACTC1* mRNA expression was correlated with methylation status at the *ACTC1* promoter region (Figure 1B, Supplementary Figure 1E) and was independent of chromosome 15 copy number (Supplementary Figure 1F). Among childhood tumors for which gene expression has been previously assessed by RNA sequencing, *ACTC1* mRNA was found to be highly expressed in SHH and WNT medulloblastoma as well as Rhabdomyosarcoma (Figure 1C). Western blot analysis confirmed the expression of ACTC1 in SHH cells (DAOY, UW228, UW426), isogenic SHH cells with Myc overexpression (UW228-Myc, UW426-Myc) and Group 3 cells (D425, D458) (Figure 1E). The highest levels of ACTC1 protein are found in the SHH subgroup cells, and the lowest in Group 3 cells. UW228 and UW426 cells express much higher levels of ACTC1 than the D425 and D458 cells (P < .01, n = 3; Figure 1D and E). Myc overexpression does not alter the ACTC1 levels in SHH medulloblastoma (Figure 1D and E).

ACTC1 Incorporates Into F-actin in SHH Medulloblastoma Cells

Immunofluorescence imaging was performed on UW426 cells to determine if ACTC1 expressed in SHH medulloblastoma cells incorporates into polymerized actin filaments. Extensive overlap was observed between the polymerized F-actin which was stained with Phalloidin and the immunolabeled ACTC1 protein (Figure 1G). To verify this finding, imaging was also performed on UW426 with stable ACTC1 overexpression (UW426-ACTC1 OE), but this time probing for the FLAG-tag of the overexpressed recombinant ACTC1 protein. Immunolabeled FLAG-tagged ACTC1 co-localized with Phalloidin stained F-actin in UW426-ACTC OE cells (Supplementary Figure 2). The results confirmed the finding that ACTC1 is a constituent of polymerized actin filaments in SHH medulloblastoma.

### ACTC1 mRNA Levels Are Upregulated During Aurora Kinase B Inhibition in SHH Cells

RNA expression profiling was performed in UW426 and UW426-Myc cells with or without exposure to Aurora kinase B specific inhibitor AZD1152-HQPA for 48 h. We sought to determine the transcriptomic changes that take place in medulloblastoma cells upon Myc overexpression, and to determine if Myc regulated gene networks are differentially expressed in response to Aurora B inhibition. Furthermore, transcriptional profiling would enable us to define the gene networks that are differentially expressed upon Aurora B inhibition in Myc overexpressing cells compared to wild-type cells. Myc overexpression in UW426 cells resulted in upregulation of gene networks involved in ribosomal biosynthesis (Figure 2A). Aurora B inhibition did not alter the transcriptional networks upregulated by Myc overexpression (Figure 2B). DNA binding genes, negative regulators of DNA binding, and regulators of multicellular organism processes (RMOP) were significantly and uniquely downregulated in Myc overexpressing cells in response to Aurora kinase B inhibition (Figure 2B). Gene networks for hypoxia response and skeletal development were identified as shared response genes to Aurora B inhibition in wild-type versus Myc overexpressing UW426 cells. The differentially expressed genes in each network with > 1 or < −1 log fold change (LogFC) and P-value <.05, which did not overlap with shared response genes were as follows: DNA binding (ID3, −1.74 LogFC) and RMOP (ACTC1, −1.95 LogFC; MYL9, −1.08 LogFC; PTGDS, −1.01 LogFC). Quantitative RT-PCR analysis of ACTC1 mRNA expression in UW426 versus UW426-Myc cells after 48 h of Aurora kinase B inhibition revealed an increase in ACTC1 mRNA abundance in UW426 cells compared to UW426-Myc, D458, and D425 cells (Figure 2C).

Overexpression of ACTC1 Protects Against Apoptosis Induced by Aurora Kinase B Inhibitor in Group 3 Cells, but not in SHH Cells Overexpressing Myc

Given the association between increased ACTC1 mRNA abundance and resistance to apoptosis induced by Aurora kinase B inhibition in SHH cells, we tested whether Group 3 cells which have low endogenous ACTC1 levels and undergo apoptosis in response to Aurora kinase B inhibition are protected from apoptosis when ACTC1 is overexpressed. ACTC1 was stably overexpressed in Group 3 cells (D458) (Figure 3A). Upon Aurora kinase B inhibition for 48 h, the ACTC1 levels remained unchanged in control and ACTC1 overexpressing cells (Figure 3A). PARP1 cleavage to the 89 kDa fragment was observed with Aurora kinase B inhibition in the control cells (D458), but was significantly reduced in the ACTC1 overexpressing cells (D458-ACTC1 OE) (Figure 3B). Aurora kinase B protein levels were not altered by ACTC1 overexpression or
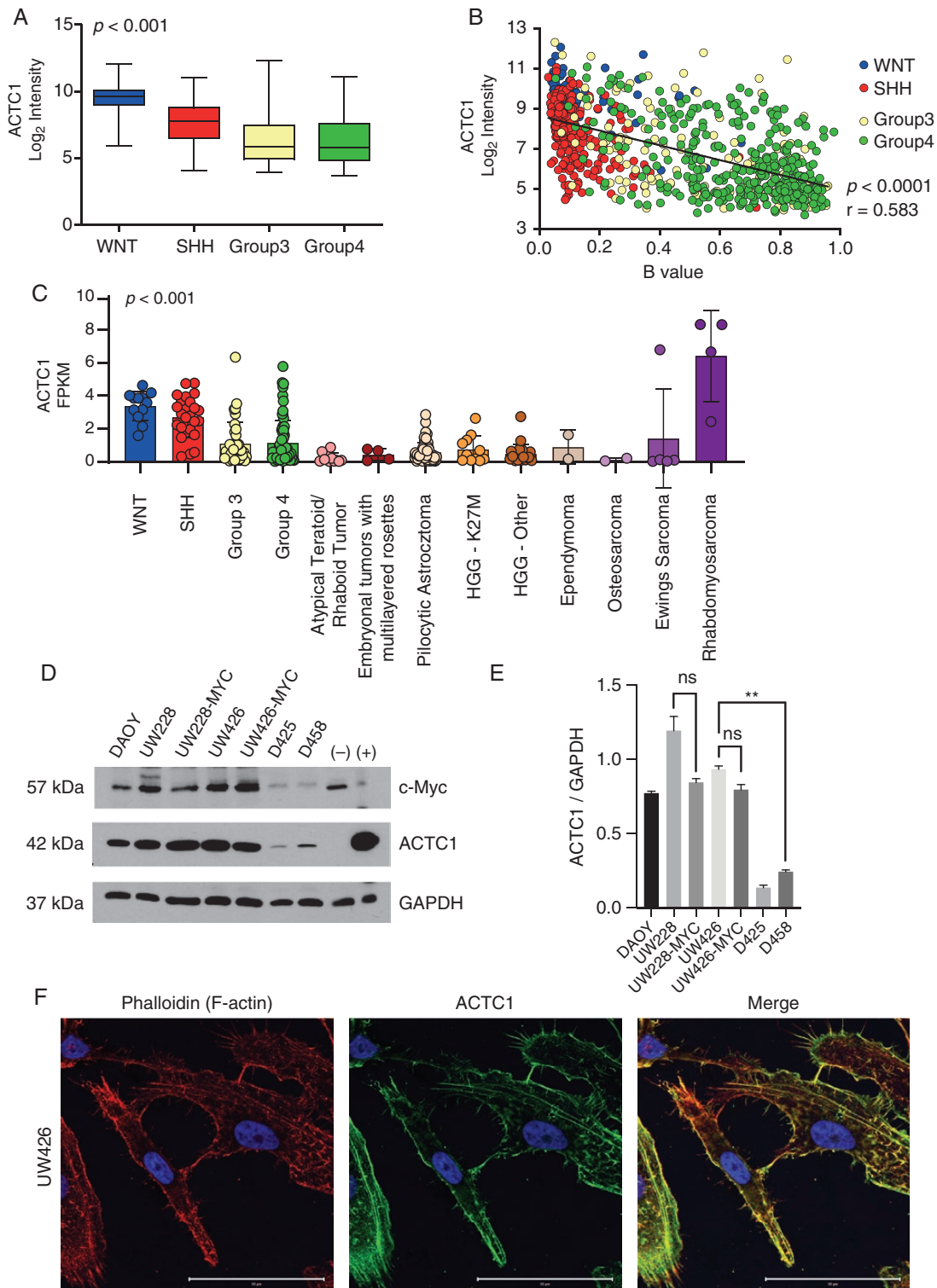
Figure 1. (A) ACTC1 mRNA expression across tumor subgroups in the Cavalli/Remke dataset (n = 763) showing increased expression in SHH and WNT tumors compared to Group 3 and 4 tumors. (B) Correlation between ACTC1 mRNA expression and promoter methylation in medulloblastoma tumors in the Cavalli/Remke dataset. (C) ACTC1 mRNA expression by RNA sequencing across multiple pediatric tumors (Pfister data set). (D) Western blot demonstrating ACTC1 and Myc expression across multiple human medulloblastoma cell lines. Positive control (+) is mouse cardiac muscle lysate and negative control (−) is mouse liver lysate. 10 μg total protein loaded. (E) Relative ACTC1 protein abundance in relation to GAPDH across human medulloblastoma cell lines. Error bars indicate standard error of the mean. **P < .005. (F) Immunofluorescence imaging of UW426 cells labeled with phalloidin (F-Actin, red) and anti-ACTC1 antibody (green). Merged image shows the red-green overlap as yellow. Scale bar is 50 μm.
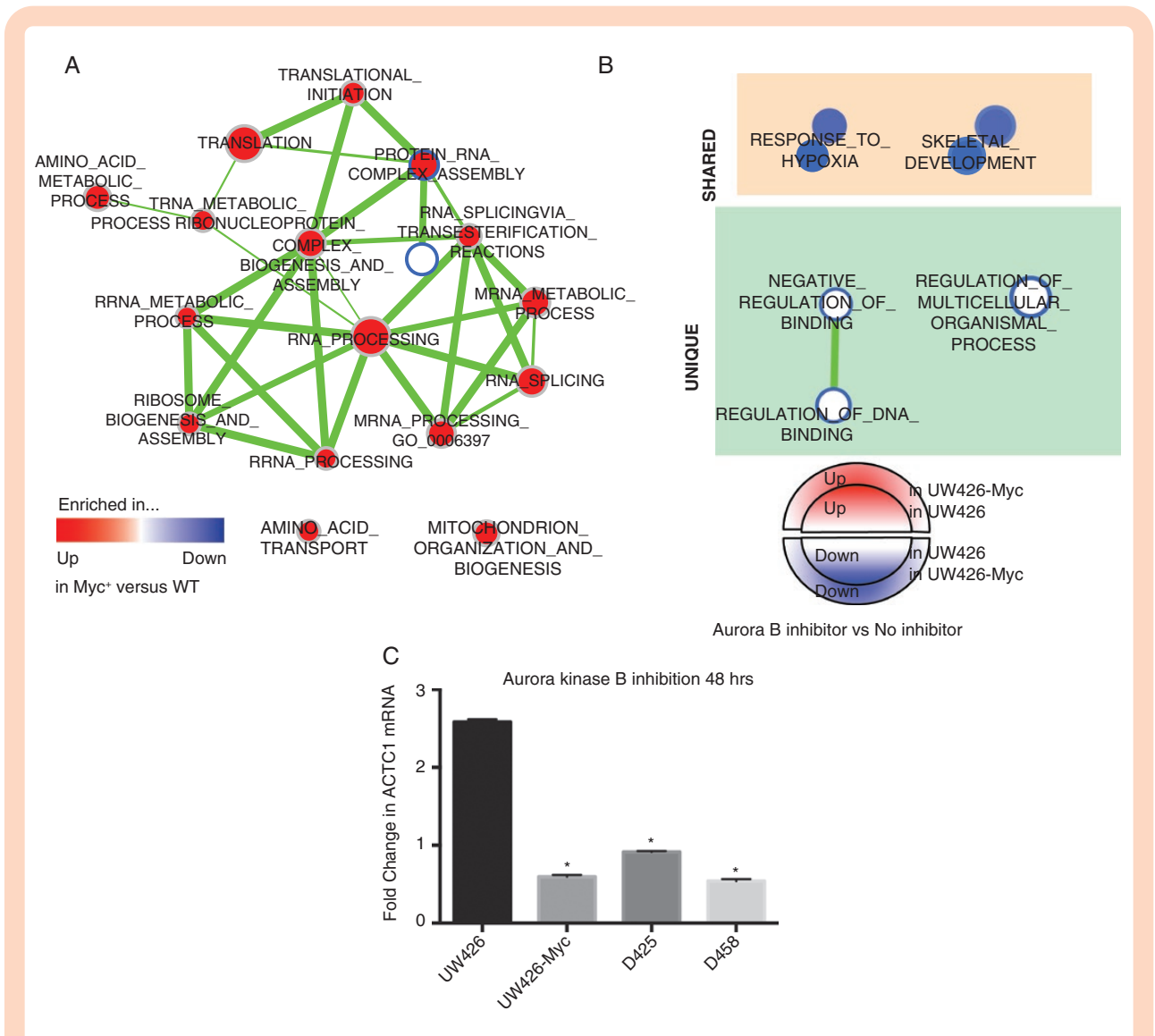
Figure 2.   (A) GO gene-set enrichment results for Myc overexpressing UW426 cells versus isogenic wild-type control. Nodes represent gene-sets and edges represent GO defined relations (Is-a, Part-of, Regulates). Gene sets that did not pass the conservative enrichment significance thresholds ($P < .001$, FDR-Q = 0.05, Overlap coefficient = 0.5) are not shown. Nodes are colored according to enrichment results: red represents enrichment in Myc overexpressing cells (ie, up-regulation due to Myc overexpression), whereas blue represents enrichment in wild-type cells (ie, down-regulation due to Myc overexpression). Color intensity is proportional to enrichment significance. Since conservative thresholds were used to select gene sets, most of the node colors are intense, corresponding to highly significant gene sets. The results indicate an overall increase in Ribosomal gene expression in Myc overexpressing cells. (B) Enrichment map displaying the enriched gene-sets in AZD1152-treated UW426 cells with endogenous Myc expression (UW426) versus Myc overexpression (UW426-Myc). Cells were treated with 100 nM AZD1152- HQPA for 48 h prior to mRNA isolation. Enrichments were mapped to the inner node area and to the node borders, respectively. Red represents enrichment in AZD1152-treated cells (ie, up-regulation after AZD1152 treatment), whereas blue represents enrichment in untreated cells (ie, down-regulation after AZD1152 treatment); color intensity is proportional to enrichment significance. Conservative threshold parameters ($P < .001$, FDR-Q = 0.05, Overlap coefficient = 0.5) were used and gene sets not meeting these thresholds are not displayed. Gene clusters that are differentially expressed uniquely in Myc overexpressing cells or shared by both wild-type and Myc overexpressing cells are outlined. Genes involved in regulation of multicellular organism process and DNA binding are uniquely downregulated in UW426 cells with Myc overexpression exposed to AZD1152 compared to UW426 cells. (C) ACTC1 mRNA expression changes in UW426, UW426-Myc, D458, and D425 cells treated with 100 nM AZD1152-HQPA for 48 h. Fold change relative to untreated cells. Bar graphs show mean fold change from 4 technical replicates per sample. Error bars are standard error of the mean, $*P < .0001$.

by Aurora kinase B inhibition in D458 cells (Figure 3B, Supplementary Figure 3A). Furthermore, overexpression of ACTC1 did not alter the protein levels of β-actin (ACTB) (Supplementary Figure 3A). Overexpression of ACTC1 in D458 cells enhanced cell viability under control conditions ($P < .0001$) and in the presence of Aurora kinase B inhibitor ($P < .0001$, Figure 3C). Thus, ACTC1 overexpression enhanced cell viability and suppressed intrinsic apoptosis that is induced by Aurora kinase B inhibition in Group 3 cells. When ACTC1 was overexpressed in SHH cells with
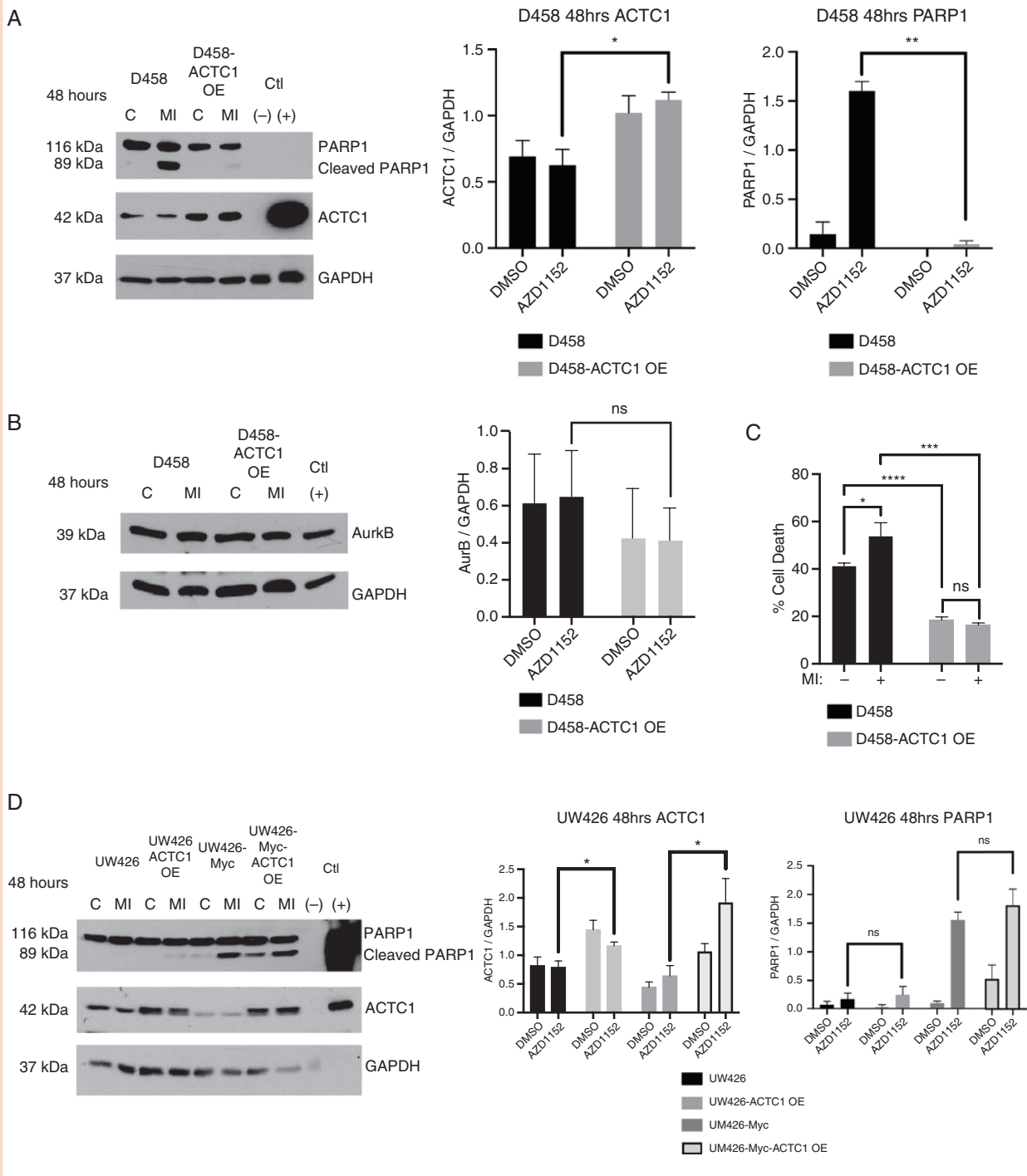
Figure 3. (A) ACTC1 and cleaved PARP1 protein expression in Group 3 cells (D458 and D458-ACTC1 OE) exposed to 100 nM AZD1152 [MI] or DMSO control [C] for 48 h, 10 µg total protein loaded. Positive control (+) is mouse cardiac muscle lysate and negative control (–) is mouse liver lysate. Data represent mean of triplicates ± SEM, *$P < .05$, **$P < .005$, ns- $P > .05$. (B) Aurora kinase B (AurkB) protein expression in Group 3 cells (D458 and D458-ACTC1 OE) exposed to 100 nM AZD1152 [MI] or DMSO control [C] for 48 h, 10 ug total protein loaded. Positive control (+) is U251 glioblastoma cell line lysate. Data represent mean of triplicates ± SEM, ns- $P > .05$. (C) Percentage of cell death determined by FACS in D458 wild-type (WT) and ACTC1-overexpressing (OE) cells after 48 h of exposure to 0.01% DMSO (–), or 100 nM AZD1152 (+). Graphs represent mean of 3 biological replicates ± SEM. *$P < .05$, ***$P < .001$, ****$P < .0001$. (D) ACTC1 and cleaved PARP1 protein expression in SHH cells (UW426, UW426-ACTC1 OE, UW426-Myc, and UW426-Myc-ACTC1 OE) exposed to 100 nM AZD1152 [MI] or DMSO control [C] for 48 h, 10 µg total protein loaded. Positive control for ACTC1 (+) is mouse cardiac muscle lysate and negative control (–) is mouse liver lysate loaded at 1 µg total protein. The PARP band in the positive control lane is a technical artifact. GAPDH is low in the control lysates due to the lower amount of protein loaded. Data represent mean of triplicates ± SEM, *$P < .05$, **$P < .005$, ns- $P > .05$.

wild-type background (UW426), there was no induction of PARP1 cleavage and the resistance to PARP1 cleavage induced by Aurora kinase B inhibition was unchanged (Figure 3D). PARP1 cleavage was induced by Aurora kinase B inhibition in SHH cells with Myc overexpression (UW426-Myc). Increased expression of ACTC1 in UW426-Myc cells did not result in suppression of PARP1 cleavage induced by Aurora kinase B inhibition (Figure 3D). ACTB and Aurora kinase B protein levels were not altered by ACTC1 overexpression or Aurora kinase B inhibition in UW426 and UW426-Myc cells (Supplementary Figure 3B). Thus, increased Myc expression bypasses the anti-apoptotic effects of ACTC1 expression in SHH medulloblastoma subjected to mitotic inhibition with Aurora kinase B specific inhibitor AZD1152-HQPA.

Reduction of ACTC1 Levels in SHH Medulloblastoma Cells Induces Apoptosis and is Synergistic with Aurora kinase B Inhibition

Knockdown of ACTC1 in UW426 and UW426-Myc cells was accomplished by transfection with plasmid DNA encoding a targeting shRNA. Out of the 3 shRNA clones tested, clone A showed the greatest knockdown in ACTC1 level and was therefore selected to be used in further experiments (Supplementary Figure 4A). The scrambled control transfected cells (UW426-ACTC1 KD sCTL and UW426-Myc-ACTC1 KD sCTL) expressed similar levels of ACTC1 as the nontransfected cells (Supplementary Figure 4A). Furthermore, the protein levels of ACTB were not changed by ACTC1 knockdown (Supplementary Figure 4B–C). ACTC1 knockdown resulted in a marked increase in PARP1 cleavage indicating activation of the intrinsic apoptosis pathway in wild-type and Myc-overexpressing UW426 cells (Figure 4A and B). The percentage of nonviable cells increased when ACTC1 was knocked down in the wild-type and Myc-overexpressing background (Figure 4C and D). Additionally, there was a greater percentage of nonviable cells when ACTC1 knockdown was combined with Aurora kinase B inhibition in both wild-type and Myc overexpressing backgrounds (Figure 4C and D).

ACTC1 Levels Control Cell Survival as Measured by Colony Formation in SHH Medulloblastoma

To assess the role of ACTC1 in promoting cell survival, a colony formation assay was performed in SHH cells (UW426) with wild-type or Myc overexpression background in which ACTC1 was knocked down by shRNA or overexpressed from a transgene. UW426 cells in which ACTC1 expression was decreased by shRNA knockdwon (UW426-ACTC1 KD) showed a 69% ± 4.0% reduction in colony formation compared to the scrambled control (P < .000001, Figure 5A). ACTC1 overexpression in UW426 cells had the effect of increasing colony formation by 70% ± 8.2% relative to control (P < .001, Figure 5A). ACTC1 knockdown impaired the colony formation capability of UW426 cells overexpressing Myc (UW426-Myc) by 51% ± 1.7% compared to scrambled control (P < .0001, Figure 5B). However, overexpression of ACTC1 in UW426-Myc cells did not augment colony formation (Figure 5B).

## ACTC1 Knockdown Inhibits Migration in SHH Cells

Given the important role of actin in cell migration, we sought to determine the effect of ACTC1 levels on SHH cell migration. Phase-contrast images were taken of a scratch assay at 0, 12, and 24-h time points with a brightfield microscope and quantitative analysis of the scratch diameter was performed. We found that the same distance was traversed by UW426 and UW426 cells transfected with scrambled control shRNA (UW426 ACTC1 KD sCTL). However, knocking down ACTC1 resulted in a marked reduction in the distance migrated in 24 h (from a total distance of 525 ± 40 μm by UW426-ACTC1 KD sCTL compared to 210 ± 32 μm by UW426-ACTC1 KD, P < .001, n = 3; Figure 6A and B).

In order to assess if knocking down ACTC1 had a similar impact on migration in SHH cells with Myc overexpression, a scratch assay was also performed with UW426-Myc and its derivatives. Knocking down ACTC1 resulted in a marked reduction in the distance migrated over the 24-h period (from 598 ± 85 μm by UW426-Myc-ACTC1 KD sCTL compared to 167 ± 33 μm by UW426-Myc-ACTC1 KD, P < .05, n = 3; Supplementary Figure 5). The overexpression of ACTC1 in both the UW426 and UW426-Myc cells, which already have elevated levels of ACTC1, did not significantly increase wound closure rate compared to their controls (Figure 6A and B, Supplementary Figure 5). These findings suggest an essential role for ACTC1 in permitting the migration of SHH cells.

ACTC1 Expression Levels Modify Stress Fiber Composition in Group 3 and SHH Cells

Stress fibers are contractile structures found in non-muscle cells that are composed of filamentous actin (F-actin) bundles, α-actinin, and non-muscle myosin II.[24] Alterations in stress fiber composition in a cell can be used to monitor changes in F-actin dynamics induced by drugs.[25] To test if ACTC1 expression has an effect on F-actin dynamics, we measured the distributions of stress fiber length in Group 3 cells (D458) with and without overexpression of ACTC1 and in SHH cells (UW426) with knockdown or overexpression of ACTC1. Notably, the histogram for stress fiber length showed a pronounced increase in the frequency of the dominant fiber length at 3 μm when ACTC1 is overexpressed in Group 3 cells (P < .01, Figure 6C). This is in keeping with an increase in total fiber length in the D458-ACTC1 OE line as compared to the wild type (Figure 6D). Conversely, in SHH cells which show high levels of endogenous ACTC1 expression, no significant increase in fiber length was observed when ACTC1 was overexpressed (Figure 6E). However, when ACTC1 was knocked down, there was a decrease in the longer fiber lengths, with a shift in the dominating fibre length from 6 to 3 μm (P < .01). Interestingly, there was an overall increase in total fiber length when ACTC1 was knocked down, which is explained by an increase in the number of the shorter stress fibers compared to the control (P < .01, Figure 6F). Thus, ACTC1 expression levels can modulate the length of actin stress fibers in medulloblastoma.
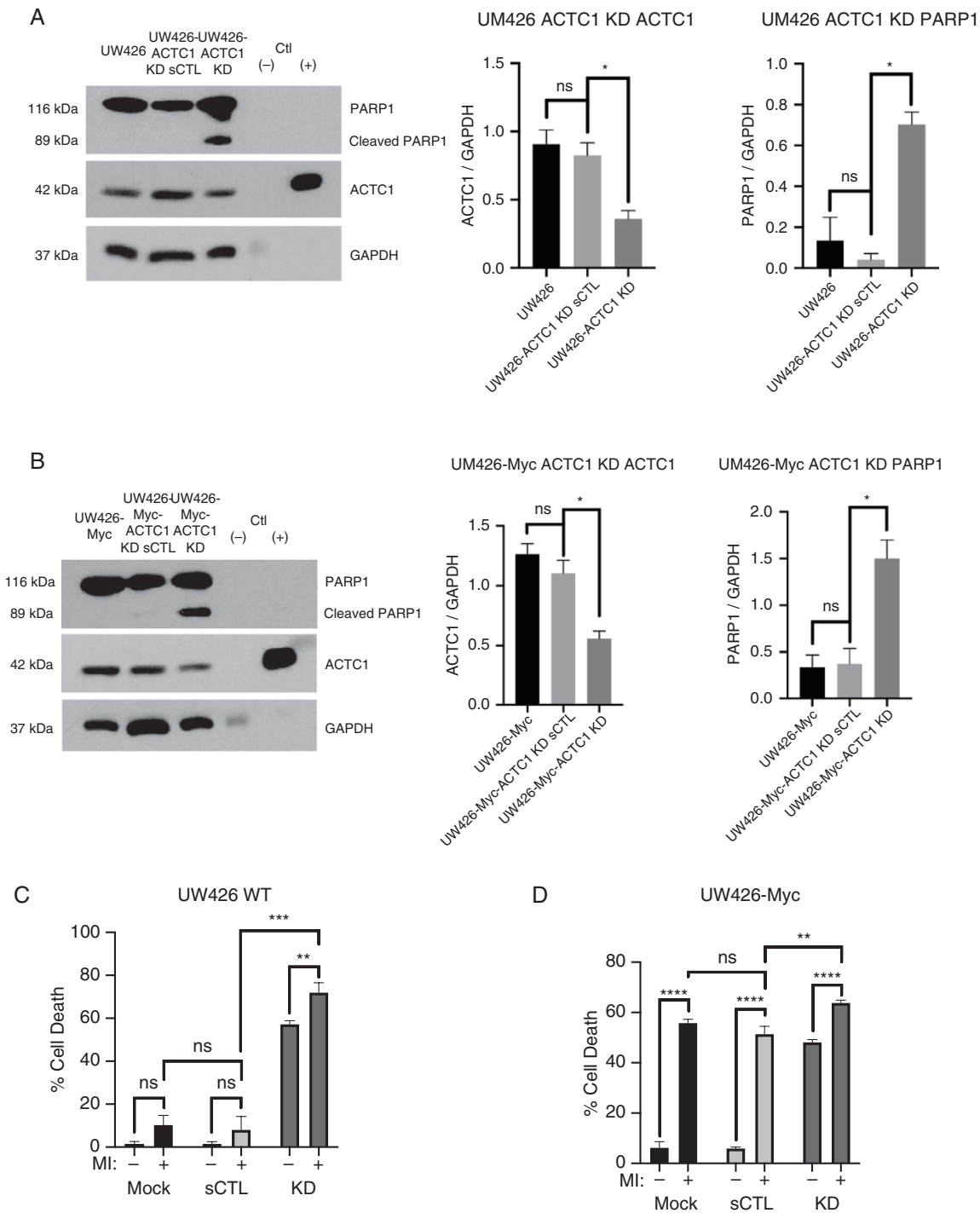
Figure 4. (A) Western blot for ACTC1 and cleaved PARP1 protein in UW426 and UW426 cells 48 h after transfection with shRNA plasmid. KD, knockdown; sCTL, scrambled control. 10 µg total protein loaded. Positive control (+) is mouse cardiac muscle lysate and negative control (−) is mouse liver lysate. Graphs represent mean of 3 biological replicates quantified by densitometry. *P < .05, ns - P > .05. (B) ACTC1 and cleaved PARP1 protein expression in UW426 cells overexpressing Myc (UW426-Myc) and overexpressing both Myc and ACTC1 (UW426-Myc-ACTC1) 48 h after transfection with shRNA plasmid. KD, knockdown; sCTL, scrambled control. 10 µg total protein loaded. Positive control (+) is mouse cardiac muscle lysate and negative control (−) is mouse liver lysate. Graphs represent mean of 3 biological replicates quantified by densitometry. *P < .05, ns - P > .05. (C) Percentage of cell death determined by FACS in UW426 cells under mock (Mock), scrambled control (sCTL) and ACTC1 knockdown (KD) shRNA transfected conditions exposed to 48 h of 100 nM AZD1152 [MI+] or 0.01% DMSO [MI-]. Graphs represent mean of 3 biological replicates ± SEM. *P < .05, **P < .01, ***P < .001, ****P < .0001, ns - P > .05. (D) Percentage of cell death determined by FACS in UW426-Myc cells under mock (Mock), scrambled control (sCTL) and ACTC1 knockdown (KD) shRNA transfected conditions exposed to 48 h of 100 nM AZD1152 [MI+] or 0.01% DMSO [MI-]. Graphs represent mean of 3 biological replicates ± SEM. **P < .01, ***P < .001, ****P < .0001, ns - P > .05.
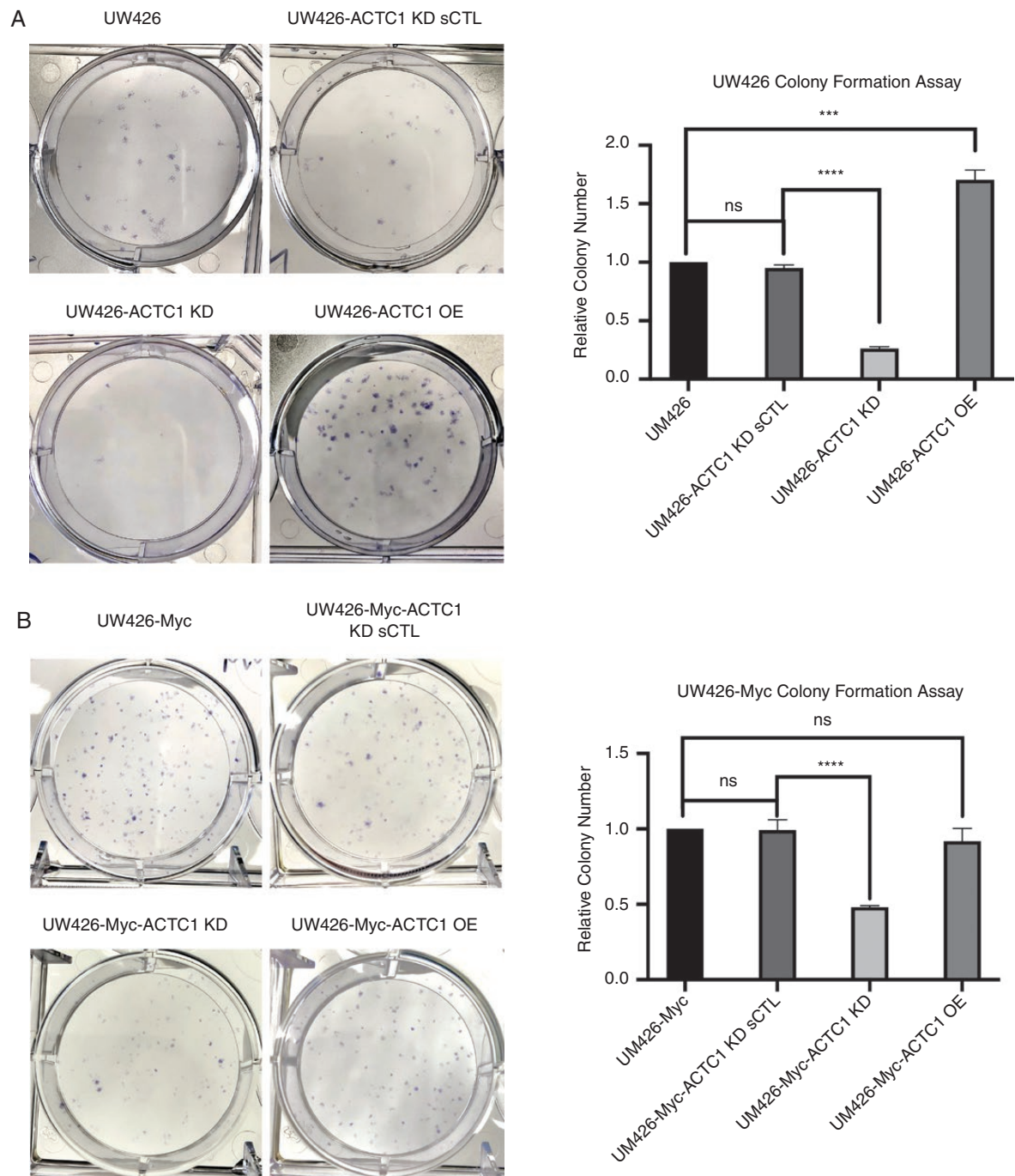
Figure 5. (A) [Left] Photographs of crystal violet stained colonies of UW426 cells with ACTC1 knockdown (KD) or overexpression (OE). sCTL, scrambled control shRNA. [Right] Quantification of colony formation in UW426 cells with ACTC1 knockdown or overexpression Graphs represent mean of 4 biological replicates ± SEM. *P < .05, ***P < .001, ****P < .0001, ns - P > .05. (B) [Left] Photographs of crystal violet stained colonies of UW426 cells overexpressing Myc (UW426-Myc) with ACTC1 knockdown (KD) or overexpression (OE). sCTL, scrambled control shRNA. [Right] Quantification of colony formation in UW426-Myc cells with ACTC1 knockdown or overexpression. Graphs represent mean of 4 biological replicates ± SEM. *P < .05, ***P < .001, ****P < .0001, ns - P > .05.

Discussion

Actin is a key structural protein in all cells and consists of Beta cytoactin and Gamma cytoactin subunits in non-muscle cells of the human body.[24] The finding of alpha cardiac actin (*ACTC1*) expression in medulloblastoma is intriguing given evidence for alternative actin isoform expression during mammalian neurodevelopment[25] and the known developmental gene expression profiles found in
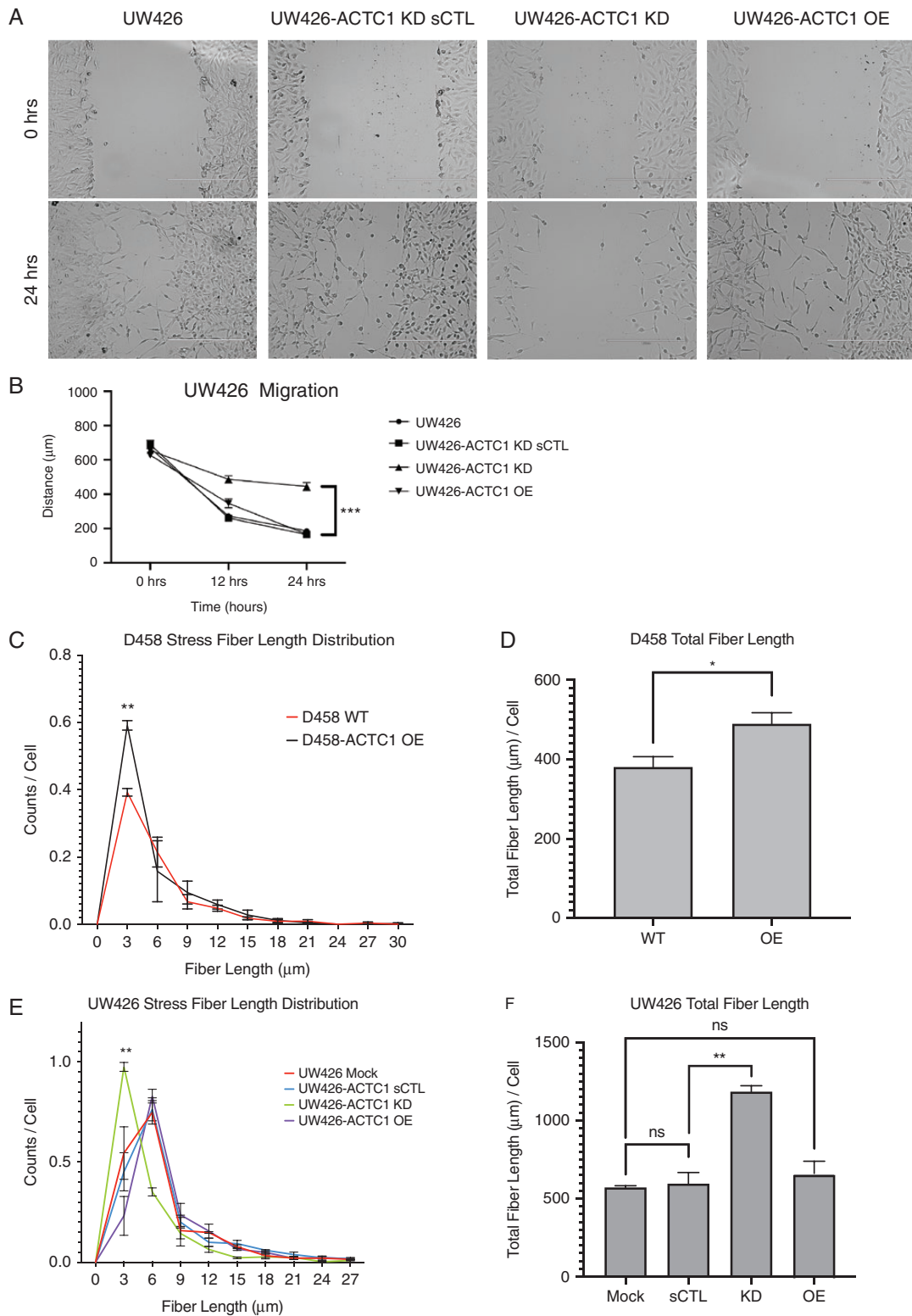
Figure 6. (A) Phase-contrast images of a scratch migration assay of UW426 cells (10× magnification) with knockdown (KD) or overexpression (OE) of ACTC1. sCTL, scrambled control shRNA. Scale bar 400 μm. (B) Graph demonstrates the wound distance over time in UW426 cells with knockdown (KD) or overexpression (OE) of ACTC1. Data represent mean of 7 technical and 3 biological replicates ± SEM, ***$P < .001$. (C) Distribution of stress fiber lengths in wild-type (WT) and ACTC1 overexpressing (ACTC1 OE) D458 cells. Counts were summed in bins of 3 μm. (D) Total stress fiber length in wild-type (WT) and ACTC1 overexpressing (ACTC1 OE) D458 cells. (E) Distribution of stress fiber lengths in wild-type (WT), ACTC1 knockdown (ACTC1 KD), ACTC1 overexpressing (ACTC1 OE) UW426 cells. Counts were summed in bins of 3 μm. (F) Total stress fiber length in wild-type (WT), ACTC1 knockdown (ACTC1 KD), ACTC1 overexpressing (ACTC1 OE) UW426 cells. Graphs C to F represent a mean of three biological replicates ± SEM. *$P<0.05$, **$P<0.01$, ns - $P>0.05$.

these tumors.[26] Furthermore, our findings of a negative correlation between *ACTC1* promoter methylation and *ACTC1* mRNA expression in medulloblastoma tumors is consistent with a report of reduced *ACTC1* gene expression in early adult mouse skeletal muscle when increased methylation is found around the transcriptional start site.[27] The analysis of *ACTC1* mRNA expression across multiple pediatric cancers revealed an association between high *ACTC1* expression and SHH pathway driven tumors (SHH medulloblastoma, WNT medulloblastoma, and Rhabdomyosarcoma). SHH medulloblastoma and Rhabdomyosarcoma are tumors that share SHH pathway activation as a common tumorigenic pathway as evidenced by formation of both of these tumors in *Ptc* +/- knockout mice.[28–31] Expression of a constitutively active Smoothened mutant in mouse endothelial progenitor cells results in aberrant expression of myogenic specification factors, including MyoD, and formation of fusion-negative Rhabdomyosarcoma.[32] Since MyoD is a known positive regulator of *ACTC1*,[33] these observations raise the possibility that ACTC1 expression may be downstream of SHH pathway activation in both SHH medulloblastoma and Rhabdomyosarcoma.

The actin cytoskeleton undergoes dramatic changes during cellular transformation resulting in altered morphology, migration ability, anchorage-independent growth, and resistance to apoptosis.[34,35] Proteins that bind to actin subunits regulate the function of actin.[36] For example, in neurons, actin dynamics regulated by actin binding proteins gelsolin and cofilin are linked to apoptosis signaling.[37,38] Actin has been actively studied as a central component of both extrinsic and intrinsic apoptotic signaling pathways.[1,34] However, the role of subunit composition and how it may alter apoptosis signaling in cancer cells is not known.

Distinct functionality of actin subunits has been observed in transgenic mouse models.[24] Three different theories for the functional uniqueness of actin subunits have been proposed based on experimental observation: (1) differing affinity for actin binding proteins, (2) difference in subcellular localization, and (3) altered F-actin function depending on the subunit mix.[24] The functional consequences of alpha-cardiac actin expression in medulloblastoma were not known prior to the work presented here. However, some recent observations in glioblastoma had suggested an important role in sensitivity to radiation and chemotherapy as well as regulation of invasion. Ohtaki et al.[16] reported that patients with glioblastoma expressing high levels of ACTC1 have shorter survival despite receiving radiation and alkylating chemotherapy. Additionally, GBMs with high ACTC1 expression show a more invasive phenotype on neuroimaging,[16] and in-vitro siRNA knockdown of ACTC1 in the U87 GBM cell line inhibited migration.[39]

We have demonstrated that medulloblastoma cells from the SHH subgroup show high ACTC1 expression and are resistant to apoptosis induced by inhibition of Aurora kinase B. The small molecule inhibitor of Aurora kinase B, AZD1152, causes G2/M arrest in medulloblastoma cells.[10] When ACTC1 is overexpressed in Group 3 cells, which normally show low ACTC1 expression, the apoptotic response to Aurora kinase B inhibition is blocked. Furthermore,

knockdown of ACTC1 in SHH MB cells increases cell death and strongly inhibits colony formation, indicating a clear functional role for ACTC1 in SHH cell survival. Interestingly, ACTC1 overexpression does not protect against apoptosis induced by Aurora kinase B inhibition in SHH cells that have been engineered to overexpress Myc. This could be explained by gene expression changes in Myc overexpressing SHH cells, that lead to alterations in actin binding proteins needed for ACTC1 mediated anti-apoptotic signaling.[10,40] Alternatively, the increased levels of ACTC1 may not be sufficient to overcome the apoptotic signaling triggered by increased entry into G2/M and excessive endoreplication in Myc-overexpressing cells.[10]

The mechanism triggering apoptosis in ACTC1 depleted cells may involve disruption of actin-binding protein binding to F-actin. Minor changes in the actin isoform forming F-actin can affect tropomyosin positioning and thereby influence interactions between F-actin and regulatory binding proteins.[41] Our observations of a marked reduction of PARP1 cleavage to the 89 kDa fragment when ACTC1 is expressed in Group 3 cells undergoing mitotic inhibition is indicative of decreased Caspase3/7 protease activity. Since Caspase 3/7 activation is downstream of loss of mitochondrial membrane potential and mitochondrial permeability transition pore formation in the intrinsic mitochondrial apoptosis pathway,[34] ACTC1 abundance in F-actin may be regulating mitochondrial membrane potential in medulloblastoma. For example, in the yeast *Neurospora crassa*, the conductance of mitochondrial voltage-dependent anion channels is differentially regulated depending on the type of actin subunit expressed.[42]

Understanding the mechanism for anti-apoptotic and migration permissive signaling mediated by ACTC1 in medulloblastoma is the key next step in elucidating the functional role of ACTC1. Immunofluorescence imaging of ACTC1 co-localizing with F-actin suggests the possibility for co-polymerization of alpha-cardiac actin with other actin subunits in medulloblastoma cells. Actin subunit co-polymerization has been previously reported *ex-vivo* for alpha-cardiac actin and skeletal muscle actin.[43] Additionally, changes in subunit composition of actin co-polymers modifies filament stability.[43] Filament stability may be important for cell survival during mitosis since cells undergoing mitosis experience increased plasma membrane tension and actively assemble a stiff actin cortex.[44–46] Localization of ACTC1 to the actin cortex in prophase (Supplementary Figure 7) further suggests a possible functional role for ACTC1 in maintaining cell integrity during mitosis. Alterations in the stability of actin filaments required for plasma membrane protrusions that function in migration could explain the significant inhibition of migration caused by ACTC1 knockdown in SHH cells. Here we have demonstrated that alteration in ACTC1 levels in medulloblastoma cells has a direct effect on stress fiber formation. The effects are cell-type dependent with overexpression of ACTC1 in Group 3 medulloblastoma resulting in a greater number of stress fibers with no change in the fiber length distribution; while knockdown of ACTC1 in SHH cells results in a shift toward shorter stress fibers and coupled with an increase total fiber formation. Stress fiber composition

is known to vary with cell type and the rigidity of the culture substrate.[47–50] In keeping with the low adhesion phenotype of D458 cells in culture, we observe shorter stress fibers in this cell line compared to UW426 cells, which adhere robustly to plastic substrate. The differences in actin subunit expression and associated stress fiber formation between Group 3 cells and SHH cells could explain the greater tendency of Group 3 tumors to show CSF dissemination at diagnosis compared to SHH tumors.[51] Further experiments to measure the polymerization properties and actin binding protein interactions of ACTC1 F-actin and as well as those of co-polymers with Beta and Gamma cytoactin subunits will help to define the cytoskeletal changes that occur when ACTC1 is expressed.

The finding that non-cell type-specific expression of ACTC1 is present in SHH medulloblastoma cells and plays a functional role in survival and migration adds to our understanding of the dynamic changes which occur in actin composition in cancer cells and their contribution to neoplastic transformation. Ultimately, this altered actin subunit expression may be a reflection of the neurodevelopmental transcriptional program that is a hallmark of SHH medulloblastoma, which is composed of cells at varying stages of granule cell precursor differentiation.[52] Interestingly, genes that contribute to structural heart development are linked to neurogenesis, including granule cell progenitor survival and differentiation.[53] The findings presented here suggest that high ACTC1 levels may serve as a biomarker for resistance to apoptosis induced by Aurora kinase B inhibition. This may extend to resistance to other mitotic inhibitors and radiation therapy, which induces G2/M arrest similar to Aurora kinase B inhibition.

Further work to understand the transcriptional regulation of ACTC1 in SHH medulloblastoma may provide insight into combination therapy that could be ultimately useful for treatment of cancers with high ACTC1 expression. Such a strategy would involve downregulation of ACTC1 and activation of apoptosis signaling through a mitotic inhibitor or radiation. ACTC1 expression is suppressed through promoter methylation[27] and activated by histone H3/H4 acetylation in non-cancer cells.[54] If a similar mechanism is involved in regulating ACTC1 expression in cancer cells, a combination of a DNA demethylase inhibitor such as C35[55] or a HDAC1 activator such as a Exifone[56] with Auora kinase B inhibition or radiation could be a potent therapy.

Conclusion

We demonstrate for the first time that alpha-cardiac actin is expressed in medulloblastoma cells. We show that alpha-cardiac actin subunit expression alters stress fiber composition and promotes SHH medulloblastoma cell survival, resistance to apoptosis, and migration. Our findings have important implications in the understanding of SHH medulloblastoma tumorigenesis and provide a novel target for therapeutic development.

Supplementary Material

Supplementary material is available at *Neuro-Oncology Advances* online.

Keywords

apoptosis | cardiac actin | chemoresistance | medulloblastoma | migration

References

1. Franklin-Tong VE, Gourlay CW. A role for actin in regulating apoptosis/programmed cell death: evidence spanning yeast, plants and animals. *Biochem J*. 2008;413(3):389-404.

2. Stehn JR, Haass NK, Bonello T, et al. A novel class of anticancer compounds targets the actin cytoskeleton in tumor cells. *Cancer Res*. 2013;73(16):5169-5182.

3. Celeste Morley S, Sun GP, Bierer BE. Inhibition of actin polymerization enhances commitment to and execution of apoptosis induced by withdrawal of trophic support. *J Cell Biochem*. 2003;88(5):1066-1076.

4. Posey SC, Bierer BE. Actin stabilization by jasplakinolide enhances apoptosis induced by cytokine deprivation. *J Biol Chem*. 1999;274(7):4259-4265.

5. Martin SS, Leder P. Human MCF10A mammary epithelial cells undergo apoptosis following actin depolymerization that is independent of attachment and rescued by Bcl-2. *Mol Cell Biol*. 2001;21(19):6529-6536.

6. Houle F, Rousseau S, Morrice N, et al. Extracellular signal-regulated kinase mediates phosphorylation of tropomyosin-1 to promote cytoskeleton remodeling in response to oxidative stress: impact on membrane blebbing. *Mol Biol Cell*. 2003;14(4):1418-1432.

7. Bunnell TM, Burbach BJ, Shimizu Y, Ervasti JM. beta-Actin specifically controls cell growth, migration, and the G-actin pool. *Mol Biol Cell*. 2011;22(21):4047-4058.

8. Pollard TD, Cooper JA. Actin, a central player in cell shape and movement. *Science*. 2009;326(5957):1208-1212.

9. Simiczyjew A, Mazur AJ, Popow-Wozniak A, Malicka-Blaszkiewicz M, Nowak D. Effect of overexpression of beta- and gamma-actin isoforms on actin cytoskeleton organization and migration of human colon cancer cells. *Histochem Cell Biol*. 2014;142(3):307-322.

10. Diaz RJ, Golbourn B, Faria C, et al. Mechanism of action and therapeutic efficacy of Aurora kinase B inhibition in MYC overexpressing medulloblastoma. *Oncotarget*. 2015;6(5):3359-3374.

11. Rivas RJ, Hatten ME. Motility and cytoskeletal organization of migrating cerebellar granule neurons. *J Neurosci*. 1995;15(2):981-989.

12. Vladoiu MC, El-Hamamy I, Donovan LK, et al. Childhood cerebellar tumours mirror conserved fetal transcriptional programs. *Nature*. 2019; 572(7767):67-73.

13. da Rocha RG, Santos EMS, Santos EM, et al. Leptin impairs the therapeutic effect of ionizing radiation in oral squamous cell carcinoma cells. *J Oral Pathol Med*. 2019;48(1):17-23.

14. Zaravinos A, Lambrou GI, Boulalas I, Delakas D, Spandidos DA. Identification of common differentially expressed genes in urinary bladder cancer. *PLoS One*. 2011;6(4):e18135.

15. Huang HC, Zheng S, VanBuren V, Zhao Z. Discovering disease-specific biomarker genes for cancer diagnosis and prognosis. *Technol Cancer Res Treat*. 2010;9(3):219-230.

16. Ohtaki S, Wanibuchi M, Kataoka-Sasaki Y, et al. ACTC1 as an invasion and prognosis marker in glioma. *J Neurosurg*. 2017;126(2):467-475.

17. Yang M, Li H, Li Y, Ruan Y, Quan C. Identification of genes and pathways associated with MDR in MCF-7/MDR breast cancer cells by RNA-seq analysis. *Mol Med Rep*. 2018;17(5):6211-6226.

18. Che CL, Zhang YM, Zhang HH, et al. DNA microarray reveals different pathways responding to paclitaxel and docetaxel in non-small cell lung cancer cell line. *Int J Clin Exp Pathol*. 2013;6(8):1538-1548.

19. Huang A, Ho CS, Ponzielli R, et al. Identification of a novel c-Myc protein interactor, JPO2, with transforming activity in medulloblastoma cells. *Cancer Res*. 2005;65(13):5607-5619.

20. Merico D, Isserlin R, Stueker O, Emili A, Bader GD. Enrichment map: a network-based method for gene-set enrichment visualization and interpretation. *PLoS One*. 2010;5(11):e13984.

21. Diaz RJ, Golbourn B, Shekarforoush M, Smith CA, Rutka JT. Aurora kinase B/C inhibition impairs malignant glioma growth in vivo. *J Neurooncol*. 2012;108(3):349-360.

22. Rogge H, Artelt N, Endlich N, Endlich K. Automated segmentation and quantification of actin stress fibres undergoing experimentally induced changes. *J Microsc*. 2017;268(2):129-140.

23. Tojkander S, Gateva G, Lappalainen P. Actin stress fibers--assembly, dynamics and biological roles. *J Cell Sci*. 2012;125(Pt 8):1855-1864.

24. Perrin BJ, Ervasti JM. The actin gene family: function follows isoform. *Cytoskeleton (Hoboken)*. 2010;67(10):630-634.

25. Goggolidou P, Soneji S, Powles-Glover N, et al. A chronological expression profile of gene activity during embryonic mouse brain development. *Mamm Genome*. 2013;24(11-12):459-472.

26. Azzarelli R, Simons BD, Philpott A. The developmental origin of brain tumours: a cellular and molecular framework. *Development*. 2018;145(10):dev162693.

27. Boutilier JK, Taylor RL, Ram R, et al. Variable cardiac alpha-actin (Actc1) expression in early adult skeletal muscle correlates with promoter methylation. *Biochim Biophys Acta Gene Regul Mech*. 2017; 1860(10):1025-1036.

28. Hahn H, Wojnowski L, Zimmer AM, Hall J, Miller G, Zimmer A. Rhabdomyosarcomas and radiation hypersensitivity in a mouse model of Gorlin syndrome. *Nat Med*. 1998;4(5):619-622.

29. Tostar U, Malm CJ, Meis-Kindblom JM, Kindblom LG, Toftgard R, Unden AB. Deregulation of the hedgehog signalling pathway: a possible role for the PTCH and SUFU genes in human rhabdomyoma and rhabdomyosarcoma development. *J Pathol*. 2006;208(1):17-25.

30. Beauchamp E, Bulut G, Abaan O, et al. GLI1 is a direct transcriptional target of EWS-FLI1 oncoprotein. *J Biol Chem*. 2009;284(14):9074-9082.

31. Wetmore C, Eberhart DE, Curran T. The normal patched allele is expressed in medulloblastomas from mice with heterozygous germ-line mutation of patched. *Cancer Res*. 2000;60(8):2239-2246.

32. Drummond CJ, Hanna JA, Garcia MR, et al. Hedgehog Pathway Drives Fusion-Negative Rhabdomyosarcoma Initiated From Non-myogenic Endothelial Progenitors. *Cancer Cell*. 2018;33(1):108-124 e105.

33. Ishibashi J, Perry RL, Asakura A, Rudnicki MA. MyoD induces myogenic differentiation through cooperation of its NH2- and COOH-terminal regions. *J Cell Biol*. 2005;171(3):471-482.

34. Desouza M, Gunning PW, Stehn JR. The actin cytoskeleton as a sensor and mediator of apoptosis. *Bioarchitecture*. 2012;2(3):75-87.

35. Suresh R, Diaz RJ. The remodelling of actin composition as a hallmark of cancer. *Transl Oncol*. 2021;14(6):101051.

36. Lee SH, Dominguez R. Regulation of actin cytoskeleton dynamics in cells. *Mol Cells*. 2010;29(4):311-325.

37. Harms C, Bosel J, Lautenschlager M, et al. Neuronal gelsolin prevents apoptosis by enhancing actin depolymerization. *Mol Cell Neurosci*. 2004; 25(1):69-82.

38. Liu T, Wang F, LePochat P, et al. Cofilin-mediated Neuronal Apoptosis via p53 Translocation and PLD1 Regulation. *Sci Rep*. 2017;7(1):11532.

39. Wanibuchi M, Ohtaki S, Ookawa S, et al. Actin, alpha, cardiac muscle 1 (ACTC1) knockdown inhibits the migration of glioblastoma cells in vitro. *J Neurol Sci*. 2018;392:117-121.

40. Bustelo XR. A transcriptional cross-talk between RhoA and c-Myc inhibits the RhoA/Rock-dependent cytoskeleton. *Small GTPases*. 2010;1(1):69-74.

41. Lehman W, Hatch V, Korman V, et al. Tropomyosin and actin isoforms modulate the localization of tropomyosin strands on actin filaments. *J Mol Biol*. 2000;302(3):593-606.

42. Xu X, Forbes JG, Colombini M. Actin modulates the gating of Neurospora crassa VDAC. *J Membr Biol*. 2001;180(1):73-81.

43. Bergeron SE, Zhu M, Thiem SM, Friderici KH, Rubenstein PA. Ion-dependent polymerization differences between mammalian beta- and gamma-nonmuscle actin isoforms. *J Biol Chem*. 2010;285(21):16087-16095.

44. Raucher D, Sheetz MP. Membrane expansion increases endocytosis rate during mitosis. *J Cell Biol*. 1999;144(3):497-506.

45. Matthews HK, Delabre U, Rohn JL, Guck J, Kunda P, Baum B. Changes in Ect2 localization couple actomyosin-dependent cell shape changes to mitotic progression. *Dev Cell*. 2012;23(2):371-383.

46. Kunda P, Pelling AE, Liu T, Baum B. Moesin controls cortical rigidity, cell rounding, and spindle morphogenesis during mitosis. *Curr Biol.* 2008;18(2):91-101.

47. Prager-Khoutorsky M, Lichtenstein A, Krishnan R, et al. Fibroblast polarization is a matrix-rigidity-dependent process controlled by focal adhesion mechanosensing. *Nat Cell Biol.* 2011;13(12):1457-1465.

48. Discher DE, Janmey P, Wang YL. Tissue cells feel and respond to the stiffness of their substrate. *Science.* 2005; 310(5751):1139-1143.

49. Herman IM, Crisona NJ, Pollard TD. Relation between cell activity and the distribution of cytoplasmic actin and myosin. *J Cell Biol.* 1981;90(1):84-91.

50. Zemel A, Rehfeldt F, Brown AE, Discher DE, Safran SA. Optimal matrix rigidity for stress fiber polarization in stem cells. *Nat Phys.* 2010;6(6):468-473.

51. Kool M, Korshunov A, Remke M, et al. Molecular subgroups of medulloblastoma: an international meta-analysis of transcriptome, genetic aberrations, and clinical data of WNT, SHH, Group 3, and Group 4 medulloblastomas. *Acta Neuropathol.* 2012;123(4):473-484.

52. Zhang L, He X, Liu X, et al. Single-cell transcriptomics in medulloblastoma reveals tumor-initiating progenitors and oncogenic cascades during tumorigenesis and relapse. *Cancer Cell.* 2019;36(3):302-318 e307.

53. Ji W, Ferdman D, Copel J, et al. De novo damaging variants associated with congenital heart diseases contribute to the connectome. *Sci Rep.* 2020;10(1):7046.

54. Wang M, Yu Q, Wang L, Gu H. Distinct patterns of histone modifications at cardiac-specific gene promoters between cardiac stem cells and mesenchymal stem cells. *Am J Physiol Cell Physiol.* 2013;304(11):C1080-1090.

55. Singh AK, Zhao B, Liu X, et al. Selective targeting of TET catalytic domain promotes somatic cell reprogramming. *Proc Natl Acad Sci USA.* 2020;117(7):3621-3626.

56. Patnaik D, Pao PC, Zhao WN, et al. Exifone is a potent HDAC1 activator with neuroprotective activity in human neuronal models of neurodegeneration. *ACS Chem Neurosci.* 2021;12(2):271-284.